Inorganic Chemistry

Article

pubs.acs.org/IC

Atom Transfer Radical Polymerization Preparation and Photophysical Properties of Polypyridylruthenium Derivatized Polystyrenes

Zhen Fang,[†] Akitaka Ito,[†] Shahar Keinan,[†] Zuofeng Chen,[†] Zoe Watson,[†] Jason Rochette,[†] Yosuke Kanai,[†] Darlene Taylor,[‡] Kirk S. Schanze,[§] and Thomas J. Meyer*[,†]

[†]Department of Chemistry, University of North Carolina, Chapel Hill, North Carolina 27599, United States

[‡]Department of Chemistry, North Carolina Central University, Durham, North Carolina 27707, United States

[§]Department of Chemistry, University of Florida, Gainesville, Florida 32611, United States

Supporting Information

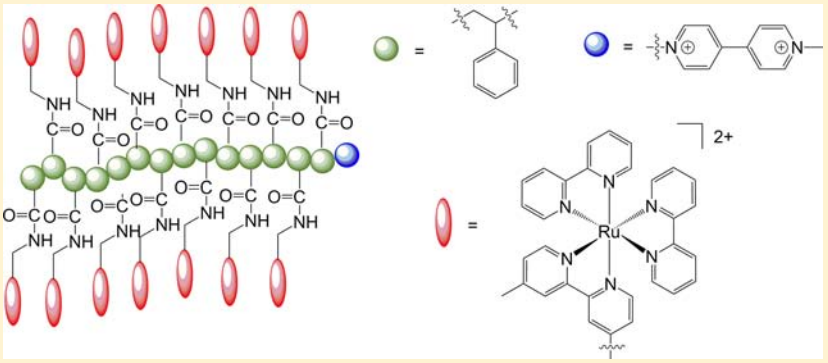

ABSTRACT: A ruthenium containing polymer featuring a short carbonyl-amino-methylene linker has been prepared by atom transfer radical polymerization (ATRP). The polymer was derived from ATRP of the N-hydroxysuccinimide (NHS) derivative of *p*-vinylbenzoic acid, followed by an amide coupling reaction of the NHS-polystyrene with Ru(II) complexes derivatized with aminomethyl groups (i.e., $[Ru(bpy)_2(CH_3\text{-bpy-}CH_2NH_2)]^{2+}$ where bpy is 2,2′-bipyridine, and CH_3-bpy-CH_2NH_2 is 4-methyl-4′-aminomethyl-2,2′-bipyridine). The Ru-functionalized polymer structure was confirmed by using nuclear magnetic resonance and infrared spectroscopy, and the results suggest that a high loading ratio of polypyridylruthenium chromophores on the polystyrene backbone was achieved. The photophysical properties of the polymer were characterized in solution and in rigid ethylene glycol glasses. In solution, emission quantum yield and lifetime studies reveal that the polymer's metal-to-ligand charge transfer (MLCT) excited states are quenched relative to a model Ru complex chromophore. In rigid media, the MLCT-ground state band gap and lifetime are both increased relative to solution with time-resolved emission measurements revealing fast energy transfer hopping within the polymer. Molecular dynamics studies of the polymer synthesized here as well as similar model systems with various spatial arrangements of the pendant Ru complex chromophores suggest that the carbonyl-amino-methylene linker probed in our target polymer provides shorter Ru−Ru nearest-neighbor distances leading to an increased Ru*-Ru energy hopping rate, compared to those with longer linkers in counterpart polymers.

INTRODUCTION

There is an ongoing interest in developing light harvesting materials that exhibit long-distance exciton and charge-transport mechanisms operating with efficiencies comparable to those found in natural photosynthetic light harvesting systems. Polymers containing transition metal chromophores are ideal targets for this objective, as they facilitate the study of photoinduced electron and energy transfer.[1−3] References therein reported on model systems involving polystyrene backbones tethered to transition metal complexes via ether or amide linkages. These studies facilitated an understanding of the mechanism and dynamics of exciton and charge transport within polymer assemblies featuring long-lived triplet metal-to-ligand charge transfer (MLCT) excited states.

In one study, with alkyl-amino-carbonyl linkages of pendant Ru(II) polypyridyl complexes to polystyrene, the average nearest neighbor distance between the periphery of Ru complexes changed by 3 Å depending on whether alternating polymer structure (**P1**, 7 Å) or homopolymer structure (**P2**, 4 Å) was used.[4] In the latter case, a dimethylene spacer between polystyrene and the amide linker enabled full loading of Ru(II) to the polymer chains, and fast energy migration on a time scale

Received: February 27, 2013
Published: July 16, 2013

   dx.doi.org/10.1021/ic400520m | *Inorg. Chem.* 2013, 52, 8511−8520

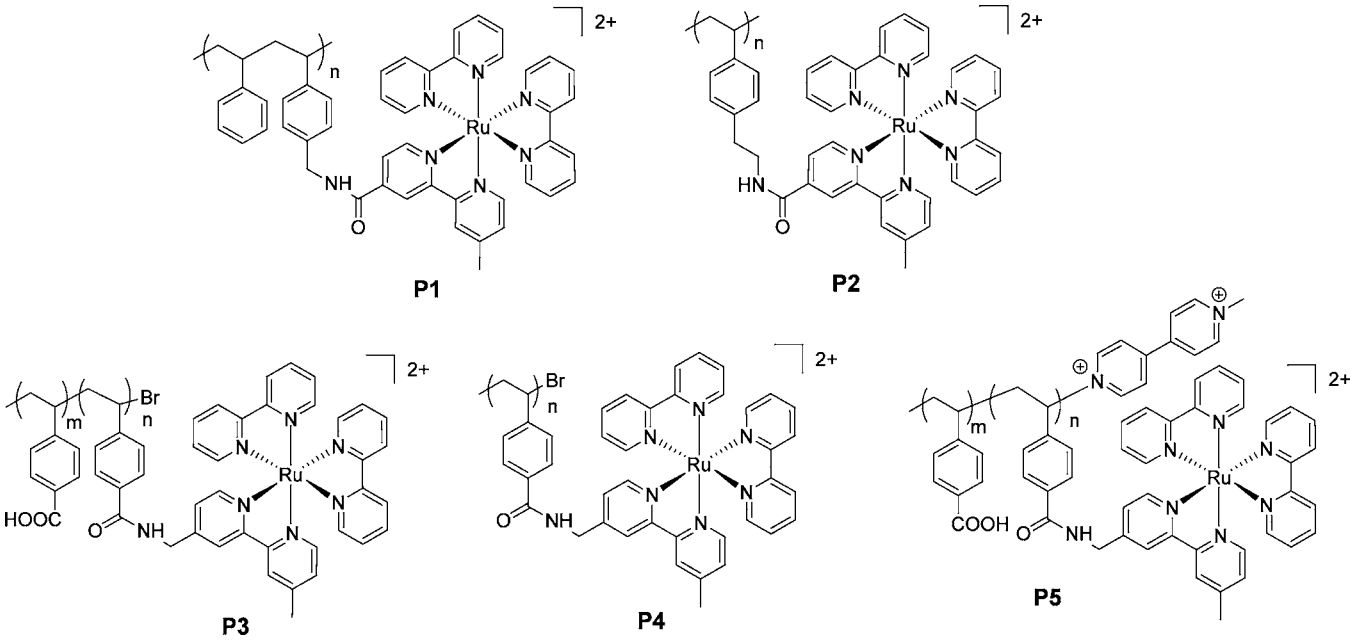

Figure 1. Structures of previously reported polypyridylruthenium derivatized polystyrenes with alkyl-amino-carbonyl linkages (**P1** and **P2**) compared with the carbonyl-amino-methylene linkages of **P3**, **P4**, and **P5**.

of nanoseconds was observed.[3] These studies and others[5] suggest that the relative spatial arrangement between the Ru(II) units is a key parameter in tuning the photophysics of these materials.

Through coordinated efforts within the Solar Fuels Energy Frontier Research Center,[6] we are investigating polystyrene based systems with very close Ru−Ru distances. To this end, the current study explores polystyrenes partly (**P3**) or fully (**P4**) derivatized by the addition of polypyridyl Ru(II) complexes based on a new carbonyl-amino-methylene linkage strategy. We report here the synthesis of these polymers prepared by atom transfer radical polymerization (ATRP). This polymerization procedure not only ensures small polydispersity indexes (PDI) and controlled chain lengths, but it also allows for incorporating halogen functional groups, notably, −Br, at the end of the polymer chain for postpolymerization modification. Application of ATRP and use of N-hydroxysuccinimide 4-vinylbenzoate provided polymers containing about 50 repeat units. Postpolymerization deprotection enabled amidation and attachment of $[Ru^{II}(bpy)_2(CH_3\text{-bpy-}CH_2NH_2)]^{2+}$ units to each polystyrene repeat unit (bpy = 2,2′-bipyridine; CH_3-bpy-CH_2NH_2 = 4-methyl-4′-aminomethyl-2,2′-bipyridine). As an additional structural feature of interest, the electron transfer *N*-methyl-4,4′-bipyridyl unit was introduced at the end of the polymer chain (structure **P5** in Figure 1) to explore its possible role in electron and energy transfer.

In these derivatized polymers an important issue is the role of local structure on intrachain dynamics. The role of the relatively short carbonyl-amino-methylene link between the polystyrene backbone and the Ru-polypyridyl units has been explored by molecular dynamic simulations on both **P3** and **P4.** Comparisons with structurally related, derivatized polymers with linkers of different lengths have provided important insights into the role of the chromophore link on interchromophore dynamics.

EXPERIMENTAL SECTION

Materials. 4,4′-Dimethyl-2,2′-bipyridine, methyl α-bromoisobutyrate, 4-vinyl benzoic acid and 1,1,4,7,7-pentamethyldiethylenetriamine (PMDETA) were purchased from Sigma-Aldrich and used without purification. Selenium dioxide, 1,4-dioxane, hydroxylamine hydrochloride, zinc, ammonium acetate, ammonia, dimethylformamide (DMF), triethylamine, and ammonium hexafluorophosphate were used as received from Fisher. Copper(I) bromide was freshly treated with acetic acid, ethanol, and acetone before use. 4′-Methyl-[2, 2′-bipyridine]-4-carbaldehyde (**1**), *N*-hydroxysuccinimide 4-vinyl benzoate (**5**) and *N*-methyl-4,4′-bipyridyl hexafluorophosphate were synthesized according to previous reports.[7,8]

The solutions for photophysical measurements were prepared in HPLC grade acetonitrile and degassed with argon for 20 min. Standard tris(2,2′-bipyridine)ruthenium(II) hexafluorophosphate $[Ru(bpy)_3](PF_6)_2$] (Figure 2) was synthesized via a counterion exchange from

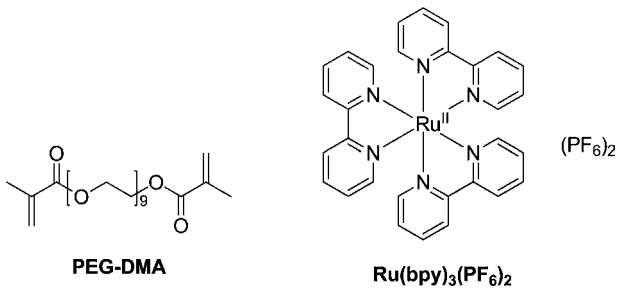

Figure 2. Structures of PEG-DMA550 and $Ru(bpy)_3(PF_6)_2$.

$Ru(bpy)_3Cl_2$. Poly(ethylene glycol)dimethacrylate with 9 ethylene glycol units (PEG-DMA550, Mn = 550) was purchased from Sigma-Aldrich. Samples in PEG-DMA550 rigid film were prepared as described in a previous report.[9]

General Methods and Instrumentation. NMR spectra were obtained on a Bruker instrument operating at 400 MHz utilizing deuterated chloroform and/or acetonitrile as solvents. Gel permeation chromatography (GPC) analysis was conducted on a Waters Alliance system composed of a 2695 Separations Module and Waters 2414 Refractive Index Detector (Waters Associates Inc., Milford, MA) using DMF as the eluent. The molecular weight was calibrated by using

dx.doi.org/10.1021/ic400520m | *Inorg. Chem.* 2013, 52, 8511−8520

polystyrene standards. IR spectra were collected on a Bruker ALPHA FT-IR spectrometer equipped with an attenuated total reflection (ATR) sampling accessory. UV−vis absorption spectra were recorded on a Hewlett-Packard 8453 spectrometer. Steady-state emission spectra were recorded on an Edinburgh Instruments FLS920 emission spectrometer, equipped with a Xenon light source. Excitation was at 460 nm, with inclusion of a 495-nm long-pass optical filter before the detector. Emission intensities at each wavelength were corrected for system spectral response. The emission quantum yields (Φ) of the complexes in CH_3CN were determined relative to $[Ru(bpy)_3](PF_6)_2$ ($\Phi = 0.095$ in CH_3CN).[10] The photon counts of the emission spectra were corrected in wavenumber scale by using an equation $I(\tilde{\nu}) = I(\lambda) \times \lambda^2$,[11] and the Φ values were calculated by using eq 1,

$$\Phi_{sample} = \Phi_{std} \frac{S_{sample}/A_{sample}}{S_{std}/A_{std}} \left(\frac{n_{sample}}{n_{std}} \right)^2 \quad (1)$$

In eq 1, the subscripts "sample" and "std" represent the sample and $[Ru(bpy)_3](PF_6)_2$, respectively, and, S, A, and n are the integrated area of the emission band, the absorbance at an excitation wavelength, and the refractive index of the solvent used. Time-correlated single photon counting data were obtained by the same instrument equipped with a pulsed, 445 nm laser source (Edinburgh Instruments EPL-445, fwhm ~1.5 ns, repetition rate = 50,000 Hz). Emission from Ru(II) complex was observed at 610 or 650 nm. Decay traces were fitted by using the Edinburgh F900 or Origin 8.1 software package.

Electrochemistry was probed by using cyclic voltammetry on a computer-controlled CHI660A electrochemical workstation, where a glassy carbon electrode served as the working electrode, a platinum electrode as the counter electrode, and an $AgNO_3$/Ag electrode as the reference. A solution of tetrabutylammonium hexafluorophosphate (0.1 M) in degassed dry acetonitrile was used as the supporting electrolyte, and the scan rate was 100 $mV \cdot s^{-1}$.

Computational Details. All structures for calculation were constructed using the Materials Studio suite (Accelrys Software Inc., San Diego, 2011). Geometries of the monomer were optimized using the B3LYP DFT functional,[12] and the Lanl2DZ basis sets,[13] as implemented in Gaussian09 version 09a02.[14] The optimization was done with "Grid = UltraFine" and "Tight" convergence criteria. The repeat units were constructed by the "Build Polymer" module in Materials Studio. Gas phase geometries of the polymers were optimized, and then annealed, using the Universal Force Field (UFF) as implemented in the Forcite module in Materials Studio,[15] with atomic charges (Mulliken charges) obtained using the QM calculations. The annealing step included 10 cycles starting at an initial temperature of 300 K and progressing to a final temperature of 500 K in a time step of 0.2 fs with 5 heating ramps per cycle and 100 molecular dynamic steps per ramp. The simulation cell was built by the "Amorphous Cell" module in Materials Studio, and it included the polymer, molecules of PF_6^- (counterions), and molecules of acetonitrile solvent. The number of acetonitrile molecules was determined by preparing a simulation cell that was 20 Å larger than the polymer in each direction with the cell density of acetonitrile (0.783 g/mL). The simulation cell was annealed using the same conditions described above for the polymer annealing. The annealed cell then went through a molecular dynamics run of 2 ns, with the canonical ensemble (NVT, constant number of atoms, constant volume, and constant temperature of 298K enabled by the Nose themostat), using a time step of 1 fs. Snapshots of the resulting structures were collected every 0.5 ps during the second ns of each molecular dynamic run, resulting in a trajectory of 2000 snapshots for analysis. Table 1 specifies all the polymers that were studied in this report. Structures of **P3′** and **P4′** are shown in the Supporting Information, both of which have replaced the carbonyl-amino-methylene linkers with carbonyl-amino-ethylene linkers.

Synthesis. 4′-Methyl-[2, 2′-bipyridine]-4-carbaldehyde Oxime (2). To a solution of **1** (2.5 g, 12.6 mmol) in methanol (30 mL) was added hydroxylamine hydrochloride (3 g, 44 mmol), K_2CO_3 (8 g, 60 mmol) and water (30 mL). The reaction mixture was stirred for 1 h at 80 °C. After cooling to room temperature, the mixture was poured into cold water (300 mL) and filtered. Recrystallization from methanol yielded **2** as a white solid (2.41 g, 90%). The ^{1}H NMR is identical to the literature.[16]

Table 1. Polymers Studied Using UFF MD

name	loading	# of repeat units	# of PF_6^- molecules	# of solvent molecules	average nearest-neighbor Ru−Ru distance/Å
P3	90%	20	36	1206	10.31 ± 1.30
P4	100%	20	40	1184	11.11 ± 1.20
P3′	90%	20	36	1203	11.68 ± 1.09
P4′	100%	20	40	1181	11.06 ± 1.09

4-Methyl-4′-aminomethyl-2,2′-bipyridine (3). A mixture containing **2** (2.13 g, 10 mmol), ammonium acetate (1.93 g, 25 mmol), ammonia (30 mL, 50 mmol), ethanol (20 mL), and water (20 mL) was heated to reflux. Zinc powder (2.8 g, 50 mmol) was added in portions over 30 min. After the reaction mixture was heated at reflux for 3 h, it was cooled and filtered to remove the zinc residue. The filtrate was concentrated to remove ethanol. NaOH (7 g) was added to form a white precipitate that changed to a slightly turbid solution. The mixture was extracted with methylene chloride (3 × 100 mL). After drying over $MgSO_4$, the solvent was removed under reduced pressure to yield a white solid (1.50 g, 75%). ^{1}H NMR (400 MHz, $CDCl_3$) δ 8.60 (d, 1H, J = 5.2 Hz), 8.53 (d, 1H, J = 5.2 Hz), 8.34 (s, 1H), 8.24 (s, 1H), 7.30 (d, 1H, J = 4.8 Hz), 7.14 (d, 1H, J = 4.4 Hz), 3.99 (s, 2H), 2.44 (s, 3H); ^{13}C NMR (100 MHz, $CDCl_3$) δ 156.31, 155.79, 153.01, 149.20, 148.85, 148.09, 124.67, 121.94, 121.89, 119.27, 45.54, 21.10. High resolution Mass, Calc. 199.1109, found, 199.1002.

$[Ru(bpy)_2(CH_3\text{-bpy-}CH_2NH_2)](PF_6)_2$ (4). A mixture containing $Ru(bpy)_2Cl_2$ (0.484 g, 1.0 mmol), **3** (0.20 g, 1.0 mmol), ethanol (5 mL), and H_2O (5 mL) was refluxed overnight in argon. Ethanol was distilled out under reduced pressure. The residue was filtered and washed with water (20 mL). To the aqueous solution, NH_4PF_6 (0.5 g, 3 mmol) was added to yield an orange solid (0.51 g, 55%). ^{1}H NMR (400 MHz, CD_3CN) δ 8.47−8.50 (m, 5H), 8.38 (s, 1H), 8.04 (t, 4H, J = 7.2 Hz), 7.72 (br, 4H), 7.60 (t, 1H, J = 5.8 Hz), 7.52 (d, 1H, J = 5.6 Hz), 7.36−7.40 (m, 5H), 7.22 (d, 1H, J = 6.0 Hz), 4.02 (s, 2H), 2.53 (s, 3H). High resolution Mass, Calc. 321.5999, found, 321.6005 ($Ru(bpy)_2(CH_3\text{-bpy-}CH_2NH_2)^{2+}$).

Precursor Polymer 6. A mixture containing **5** (0.368 g, 1.5 mmol), methyl α-bromoisobutyrate (4 μL), PMDETA (42 μL), and dimethylsulfoxide (DMSO, 0.5 mL) was degassed via three freeze−pump−thaw cycles. CuBr (4 mg, 0.028 mmol) was added to the mixture under argon flow. The reaction mixture was warmed to 80 °C and stirred overnight under argon. The green mixture was poured into methanol (20 mL) to yield a solid. The solid was filtered and dissolved in DMF. The DMF solution was passed through a short neutral alumina column to remove the copper residue. The solution was then concentrated and precipitated from methanol to yield a white solid (82 mg, 22%). M_n: 1.3 × 10^4, PDI: 1.2; IR (cm^{-1}): 2936 (C−H, phenyl), 1773 (carbonyl, imide), 1732 (carbonyl, C(ON)═O), 1204 (C−N, imide); ^{1}H NMR (DMSO-d6, 400 MHz) δ 7.83, 6.82, 4.40, 2.85, 1.52.

P3. To a solution of **6** (20 mg, 0.081 mmol) in anhydrous DMF (3 mL), triethylamine (0.1 mL, 0.72 mmol) and **4** (80 mg, 0.089 mmol) were added. After stirring at 40 °C for 2 days, the solution was concentrated and poured into a methanol/H_2O mixture (50:10 mL). The mixture was centrifuged and washed with methanol (20 mL × 5) until a colorless filtrate was obtained. The resulting orange solid was isolated as product (28 mg, 75%). IR (cm^{-1}): 3422 (O−H, carboxylic acid), 3083 (N−H, amide); 2924 (C−H, phenyl), 1708, 1659 (carbonyl, amide); ^{1}H NMR (DMSO-d6, 400 MHz) δ 8.83, 8.15, 7.71, 7.52, 7.34, 6.57, 4.66, 1.55.

P5. To a solution of **P3** (5 mg) in CH_3CN (5 mL), *N*-methyl-4,4′-bipyridyl hexafluorophosphate (10 mg) was added. After refluxing overnight, the solution was concentrated and poured into methanol/hexane (20:20 mL) to yield a precipitate. The precipitate was washed with 1:1 methanol/hexane (20 mL × 3) until no *N*-methyl-4, 4′-bipyridyl hexafluorophosphate was visually observed under a 254 nm UV lamp. The slurry cake was dried in vacuum to yield a yellow solid

dx.doi.org/10.1021/ic400520m | Inorg. Chem. 2013, 52, 8511−8520

Scheme 1

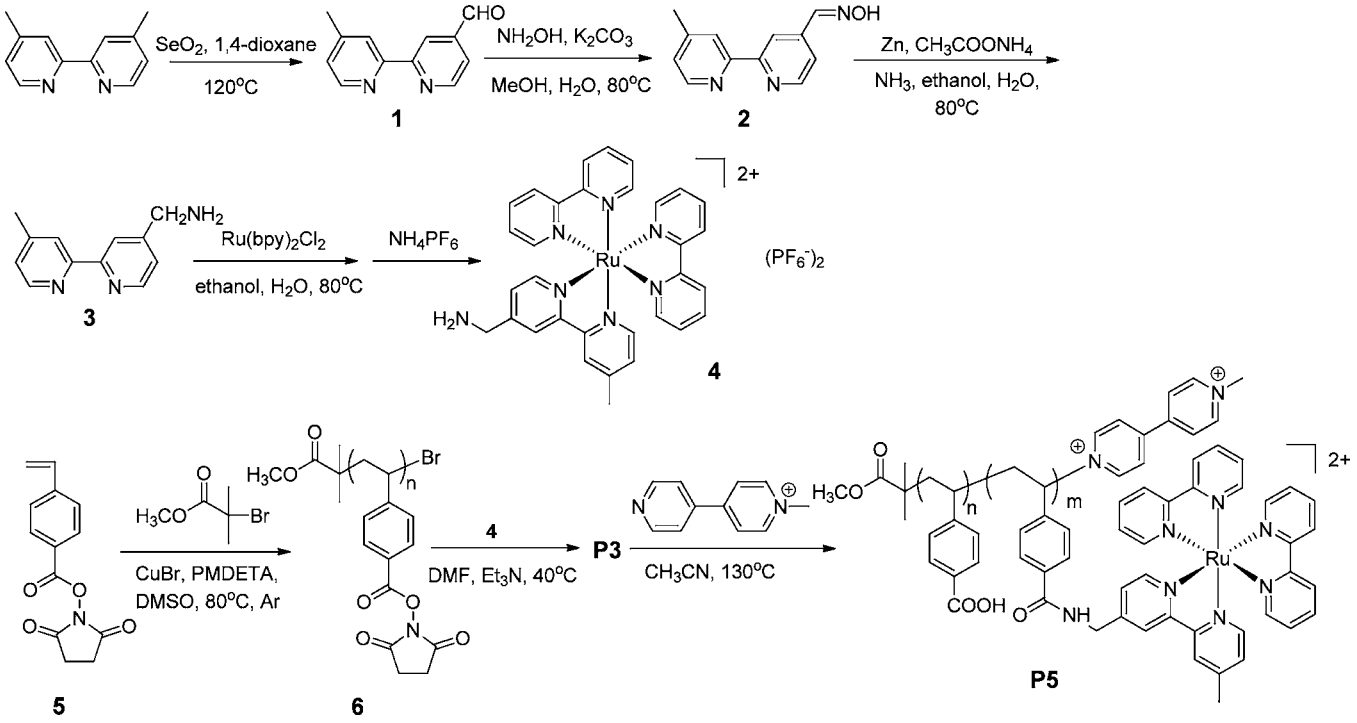

(4 mg, 79%). IR (cm^{-1}): 3420 (O−H, carboxylic acid), 3081 (N−H, amide); 2922 (C−H, phenyl), 1702, 1654 (carbonyl, amide); ^{1}H NMR (DMSO-d6, 400 MHz) δ 8.48, 8.35, 8.02, 7.71, 7.53, 7.37, 6.60, 1.44.

RESULTS AND DISCUSSION

Synthesis and Characterization. Our group has developed several polymerization strategies to prepare functionalized polystyrenes, which can be further modified by attaching Ru or Os complexes.[3,4] A living anionic polymerization of silane-protected amine derivatized styrene afforded polymers with narrow PDI and controlled molecular weight. However, because of the strongly basic conditions used for anionic polymerization, the reaction is not particularly functional group tolerant, limiting the scope of the types of functional monomers that can be used. We also recently developed reversible addition−fragmentation chain transfer (RAFT) polymerization combined with the azide-alkyene click chemistry for preparing polypyridine Ru(II)-derivatized polystyrenes.[5c] Unfortunately, the −SH end-group arising from the RAFT initiator quenches the MLCT state by a charge transfer mechanism, leading to considerable reduction in the lifetime of the MLCT state, especially in short chain length polymers. In comparison, the ATRP technique catalyzed with copper(I) affords an effective method to achieve polymers with narrow PDI and no thiol end-group functionality. Meanwhile, the bromide functional end group present in the ATRP polymer makes it possible to create block copolymers or chain terminated nanoparticles for further derivatization.[17]

Scheme 1 shows the synthetic route for the target polymers. In the first step, 4,4′-dimethyl-2,2′-bipyridine was selectively oxidized to the monoaldehyde by SeO_2, followed by the formation of oxime. The oxime is then reduced by zinc in a weakly basic medium. Using a typical Ru complex preparation method,[18] Ru monomer **4** was synthesized in moderate yield. Polymer precusor **6** was prepared from *N*-hydroxysuccinimide 4-vinylbenzoate in the presence of methyl α-bromoisobutyrate as the initiator by a typical ATRP procedure. GPC measurements on the product show that polymer **6** has a number average molecular weight (M_n) of 1.3×10^4 g/mol with a PDI of 1.2. The small PDI is a characteristic of ATRP and controlled radical polymerization. A typical GPC elution curve of **6** is shown in the Supporting Information, Figure S1. The degree of polymerization (DP) is calculated as the ratio of M_n to the formula weight of monomer **5**. The value obtained (DP ∼ 50) is in good agreement with the loading ratio of monomer to initiator, consistent with controlled polymerization by ATRP. As shown in the Supporting Information, Figure S2, the ^{1}H NMR spectrum of **6** features broad resonances at δ 7.8, 6.8, and 1.5 ppm, consistent with the polystyrene structure. The protons for the 2,5-dioxopyrrolidine (NHS-ester) group are located at δ 2.85 ppm. A weak resonance at 4.40 ppm is attributed to the terminal chain proton at the carbon next to the bromine atom.

The amidation reaction from **6** to **P3** was conducted in DMF with a catalytic amount of triethylamine to expedite the exchange. At the end of the reaction, copious amounts of methanol were added to remove excess free Ru complexes. The NMR spectrum of **P3** is shown in Supporting Information, Figure S2, with the proton resonances characteristic of the 2,5-dioxopyrrolidine group absent. New resonances in the aromatic region δ ∼7.5−9.0 ppm corresponding to the protons of bipyridine ligands of the Ru complex are present. A loading level of ∼90% Ru on the polystyrene repeat units is estimated based on the integration ratio of aromatic to alkyl protons. The unsubstituted NHS ester groups are hydrolyzed to carboxylic acids under the amidation reaction conditions and workup, as confirmed by FTIR as discussed below. The functionalization of the **P3** end group (-Br) with *N*-methyl-4,4′-bipyridinium hexafluorophosphate (MV^+ PF_6^-) was confirmed by ^{1}H NMR. After thoroughly washing the crude product with a 1:1 methanol/hexane mixture until no MV^+ PF_6^- is observed in the filtrate, **P5** is obtained as a yellow solid. Although NMR

dx.doi.org/10.1021/ic400520m | Inorg. Chem. 2013, 52, 8511−8520

shows no significant change in the aromatic region, the resonances at 4.66 ppm attributed to −CHBr in the spectrum of **P3** are absent in that of **P5** because of the replacement of −Br by *N*-methyl-4,4′-bipyridinium.

The amidation reaction of **6** to **P3** was monitored by FT-IR as well (Supporting Information, Figure S3). The spectrum of poly(4-vinyl benzoic acid) (abbreviated as **PSCOOH**) is shown for comparison. The phenylene unit of polystyrene shows stretching bands at ∼2930 cm^{-1} for all polymers. Distinct carbonyl region bands are present in the spectra of all three polymers. In particular, an intense band in the spectrum of **6** at 1730 cm^{-1} is shifted to 1660 cm^{-1} in **P3**. This feature arises from the carbonyl stretching mode of the imide in **6** which is transformed to an amide group in **P3**. A new band appears at 3080 cm^{-1} due to the N−H stretching mode of the secondary amide in **P3**. Compared to the spectrum of **PSCOOH**, **P3** displays features consistent with some residual −COOH units in the infrared spectrum. For example, a broad band at 3420 cm^{-1} in **P3** appears for the O−H group, which features typical stretching characteristics of −COOH in **PSCOOH**. Also, the band at 1710 cm^{-1} in **P3** features an intense band from the C═O stretching mode of a −COOH group, as shown in the spectrum of **PSCOOH**.

Electrochemistry. The electrochemical properties of $[Ru(bpy)_3](PF_6)_2$, **P3**, and **P5** were studied by cyclic voltammetry (CV). As shown in Figure 3, $[Ru(bpy)_3](PF_6)_2$ and both

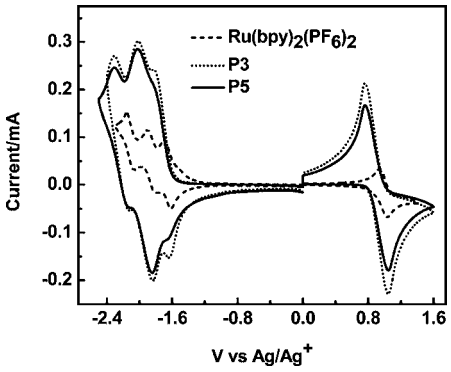

Figure 3. Cyclic voltammogram of $[Ru(bpy)_3](PF_6)_2$, **P3**, and **P5** in 0.1 M Bu_4NPF_6 in deoxygenated CH_3CN with a scan rate of 100 mV s^{-1}.

polymers feature a reversible anodic wave at ∼0.92 V vs $AgNO_3$/Ag, attributed to the Ru(III/II) couple. $[Ru(bpy)_3](PF_6)_2$ exhibits three reversible cathodic waves at −1.64, −1.86, and −2.12 V vs $AgNO_3$/Ag, from sequential one-electron reduction of each of the three bipyridine ligands. In CVs of the two polymers, anodic−cathodic peak separations, 300 mV at 100 mV/s, were observed likely resulting from slow diffusion and multiple electron transfer. However, qualitatively the polymers exhibit similar oxidation and reduction potentials compared to $[Ru(bpy)_3](PF_6)_2$. These results suggest that there is no significant interaction between the ligands at adjacent Ru sites, which is in agreement with the observation in absorption and emission described below. We also note the absence of a clearly resolved wave because of reduction of the terminal MV^{2+} unit in **P5**. The absence of a definable signal is not surprising, given that the MV^{2+} end-group is present at a ∼50-fold lower concentration than the pendant Ru(II) units.

Photophysical Properties in Solution. The absorption and emission spectra of monomer **4**, **P3**, **P5**, and $[Ru(bpy)_3](PF_6)_2$ in CH_3CN are shown in Figure 4. All solutions show MLCT absorption bands at $\lambda \sim 450$ nm, which is typical for Ru-polypyridine complexes. There is a slight red-shift (∼6 nm, 161 cm^{-1}) in the band maximum for **4**, **P3**, and **P5** compared with $[Ru(bpy)_3](PF_6)_2$. The red-shifts for **4**, **P3**, and **P5** are a consequence of the substituent effects of the electron donating methyl and aminomethyl groups in the ancillary ligand.[19] The emission maxima of **4**, **P3**, and **P5** exhibit similar red-shifts (∼11 nm, 226 cm^{-1}) compared to $[Ru(bpy)_3](PF_6)_2$. In comparing the emission quantum yields it can be seen that **P3** has a quantum yield (Φ = 0.08) that is comparable to that of monomer **4** (Φ = 0.09).

It is well-known that association of polyelectrolyte strands occurs and varies with the nature of polymer backbone,[20] counterions,[21] solvent environment,[22] and addition of electrolytes or surfactants.[23] To examine the possible impact of association on photophysical properties, a concentration dependent study was undertaken for **P3**. Within the concentration range of 5 μM to 50 μM, **P3** exhibits identical absorption and emission spectra when corrected for the concentration dependence of absorption and intensity (see Supporting Information, Figure S4). Similarly, the excitation spectrum of **P3** in acetonitrile exhibits a smooth and symmetrical pattern which mirrors the emission spectrum (see Supporting Information, Figure S5). Taken concentration dependent and excitation spectra together, the fact that the absorption and emission spectra of **4** and **P3** are essentially identical indicates that the metal complex chromophore units in **P3** are dispersed as *single* molecules without substantial aggregation or strong interchromophore interaction. A detailed discussion about polymer structure is presented in the modeling calculation section below.

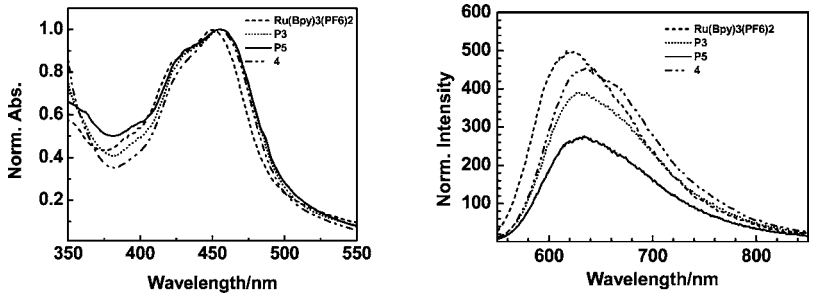

Figure 4. Absorption (left) and corrected emission spectra (right) of $Ru(bpy)_3PF_6$, monomer **4**, polymer **P3**, and **P5** in CH_3CN (λ_{ex} = 460 nm; [Ru] ∼ 10 μM.). The emission spectra have been normalized based on the absorbance at 460 nm, and the absolute intensities reflect the emission quantum yields.

dx.doi.org/10.1021/ic400520m | *Inorg. Chem.* 2013, 52, 8511−8520

The ability of MV^{2+} to oxidatively quench the MLCT excited state of $[Ru(bpy)_3]^{2+}$, resulting in efficient emission quenching, is well-established. Stern–Volmer emission quenching shows that the electron transfer quenching process is diffusion-controlled, and transient absorption spectroscopy confirms that the quenching produces the reduced acceptor, $MV^{+\bullet}$.[24] In the present work, we examined the effect of MV^{2+} on the emission of the polymeric RuL_3^{2+} chromophores in **P3** by adding *N*,*N*′-dimethyl-4,4′-bipyridyl hexafluorophosphorate ($MV(PF_6)_2$) to solutions of **P3** (Figure 5).

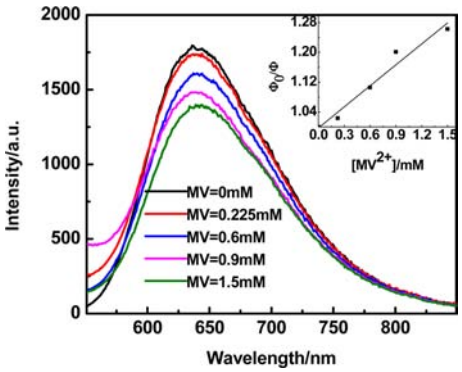

Figure 5. Emission spectra of **P3** ([Ru] = 10 μM) in the presence of MV^{2+} in deaerated acetonitrile. Inset illustrates the Stern–Volmer plot (Φ_0/Φ vs $[MV^{2+}]$), constructed by monitoring the emission intensity at 460 nm excitation.

Figure 5 illustrates the results of a typical quenching study where **P3** ([Ru] = 10 μM) was quenched by the addition of MV^{2+} with emission quenching reaching 20% upon the addition of about 1.0 mM MV^{2+}. (Note that this concentration corresponds to ~1:100 ratio of Ru chromophores to MV^{2+}.) At 1.5 mM MV^{2+} the emission maximum of **P3** red-shifted by 4 nm (81 cm^{-1}) and absorption spectra of the solution mixtures exhibited scattering at longer wavelength (>700 nm, Supporting Information, Figure S6), suggesting that MV^{2+} induces a change in polymer conformation, or possibly leads to aggregation arising from the high ionic strength. These results are supported by dynamic light scattering experiments that reveal that the hydrodynamic radius of **P3** increased from 100 to 150 nm upon the addition of MV^{2+} (see Supporting Information, Figure S7). An emission quenching study by adding $LiClO_4$ into **P3** solution shows that increasing the ionic strength impacts both emission maxima and quantum yields because of enhanced aggregation (see Supporting Information, Figure S8). A linear fit to the emission quenching data of **P3** at MV^{2+} concentrations <0.9 mM yielded $K_{SV} \sim 2.6 \times 10^2$ M^{-1}, which is 1 order of magnitude smaller than that for $[Ru(bpy)_3](PF_6)_2$ ($K_{SV} \sim 2.1 \times 10^3$ M^{-1}).[16] The reduced quenching efficiency for the polymer relative to the monomeric complex is likely due to increased electrostatic repulsion between the polycation and the cationic MV^{2+} quencher ion.

Time-correlated single photon counting (TCSPC) was applied to time resolve the decay of the ^{3}MLCT* states following excitation in the absence and presence of MV^{2+}. Multiphoton effects are unimportant at the low excitation irradiances used in the TCSPC experiments (~ nJ/pulse).[5b] Thus, herein emission decay studies were able to further probe the quenching mechanism of MV^{2+} on the MLCT excited state decay kinetics for the polymeric chromophores. Thus, emission decays of **P3** were monitored at 610 nm as a function of MV^{2+} concentration. As shown in Figure 6a, addition of MV^{2+} slightly alters the decay kinetics. A biexponential fit to the emission decay afforded median lifetimes (τ) that were subsequently used to construct a lifetime vs concentration of added MV^{2+} plot (Figure 6b), where the biexponential fitting results in reasonable reduced R^2 (~0.997–0.998 for the 5 decays). This plot is similar to one derived from the quantum yield quenching plot (Φ_0/Φ vs $[MV^{2+}]$), suggesting the emission quenching of **P3** by MV^{2+} is dynamic.

As described above, polymer **P5** results from the substitution of the -Br end-group in **P3** with the MV^{2+} electron acceptor unit at the terminus. As shown in Figure 4, the absorption and emission maxima of **P5** are essentially indentical to those of **P3**, indicating that the presence of the MV^{2+} end-group does not strongly influence the properties of the Ru chromophores. However, interestingly we find that the emission quantum yield of **P5** (Φ = 0.054) is reduced by approximately 30% relative to that of **P3**, suggesting that the MV^{2+} end-group is active as an intrachain quencher of MLCT excited states. Given that the DP value of **P5** is ~50, the approximate Ru: MV^{2+} ratio in the polymer chains is 50:1. Thus for a solution in which the **P5** polymer repeat unit concentration is 10 μM (e.g., [Ru] = 10 μM), the approximate concentration of the MV^{2+} end-groups is 0.2 μM. In this system, we see 30% emission quenching corresponding to an effective Stern–Volmer quenching constant of ~2.1×10^6 M^{-1} which is 10,000-fold more efficient in the **P3**/MV^{2+} bimolecular quenching system. The efficient quenching by the MV^{2+} end-group in **P5** suggests that there is an active channel by which MLCT excitons can migrate among

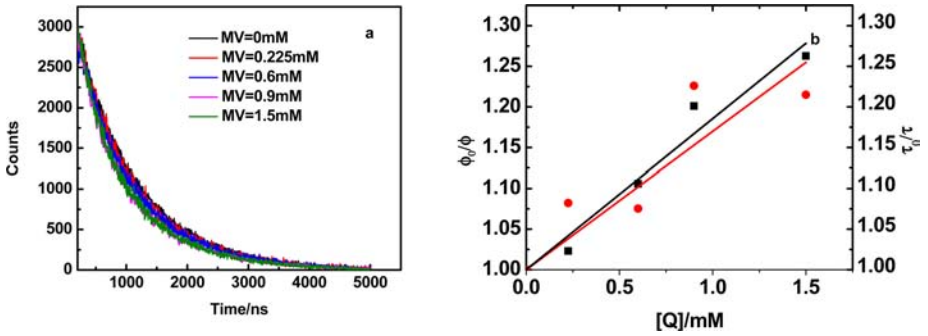

Figure 6. (a) Emission decay of **P3** (λ_{ex} = 445 nm, λ_{em} = 610 nm) and (b) Stern–Volmer plot for emission quantum yield quenching (Φ_0/Φ, black square, λ_{ex} = 460 nm), and median lifetime decay (τ_0/τ, red circle, λ_{ex} = 445 nm, λ_{em} = 610 nm) in the presence of MV^{2+} in degassed acetonitrile solution.

dx.doi.org/10.1021/ic400520m | Inorg. Chem. 2013, 52, 8511–8520

the pendant Ru sites in the polymer. This type of intrachain exciton migration has been well-documented in previous studies of polystyrenes that contain pendant Ru-chromophores, where the mechanism has been attributed to MLCT exciton transport by a site-to-site hopping mechanism.[3,5]

In general, small molecules including $Ru(bpy)_3(PF_6)_2$ and monomer **4** show single exponential emission decay kinetics, while **P3** and **P5** feature multiple exponential decays as shown in Figure 7. Individual decay profiles are shown in the

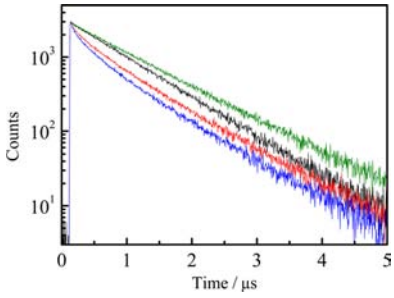

Figure 7. Emission decay profiles of $Ru(bpy)_3(PF_6)_2$ (black), monomer **4** (green), **P3** (red), and **P5** (blue) in CH_3CN: excitation wavelength = 445 nm and emission wavelength = 610 nm. [Ru] ~ 50 μM.

Supporting Information, Figure S9. The emission lifetimes of $Ru(bpy)_3(PF_6)_2$ and **4** were determined to be ~800−900 ns, typical for Ru-polypyridine complexes (Table 2).[25] On the

Table 2. Emission Decay of $Ru(bpy)_3(PF_6)_2$, 4, P3,, and P5 in CH_3CN

compounds	τ/ns[a]	$\langle\tau\rangle$/ns
$Ru(bpy)_3(PF_6)_2$	806	
4	945	
P3	τ_1 = 281 (0.33); τ_2 = 808 (0.67)	634
P5	τ_1 = 82 (0.19); τ_2 = 393 (0.43); τ_3 = 900 (0.38)	527

[a]Note: Number in parenthese is the fraction amplitude of the decay components.

other hand, **P3** and **P5** exhibit short-lived decay components in addition to relatively long-lived components typical of the isolated ruthenium chromophores. The rapid decay component is due to energy migration by Ru* to Ru hopping to low energy sites on the polymer which undergo rapid decay as has observed in previous studies.[3] When the polymer is end-capped with MV^{2+} in **P5**, the electron trap site introduces an additional ~80 ns component compared to **P3** arising from energy transfer to the terminus and being oxidatively quenched.

Photophysics in Rigid Medium. To obtain additional evidence for intrastrand energy migration, we conducted photophysical measurements on **P3** in a semirigid polymer film. Since the MLCT excited states in the Ru complexes are sensitive to the local environment, a distribution of excited state energies and dynamics exists along an individual polymer strand. In a homogeneous solution environment solvent fluctuations lead rapid redistributions of local environments while local environments are, at least, partly frozen in polymer films. To explore the role of the film environment on energy decay dynamics and time-resolved emission, the polymers were dispersed in rigid PEG-DMA550 films. The samples were prepared by using a literature procedure; with 2,2′-azobis(2,4-dimethylvaleronitrile) (Vazo 52 from DuPont) as the thermal polymerization initiator.[9] The solid state film described here is different from a neat film formed by casting, spraying, or dipping because the polymer is diluted in a film free of interstrand interactions. Both intermolecular and intramolecular energy transfer typically play role in neat films. In the diluted PEG-DMA films photophysical properties are dominated by intrastrand events and the distribution of excited state energies and dynamics for individual polymer strands.

Figure 8 compares the steady-state absorption and emission spectra of **P3** in CH_3CN and PEG-DMA550 films. The

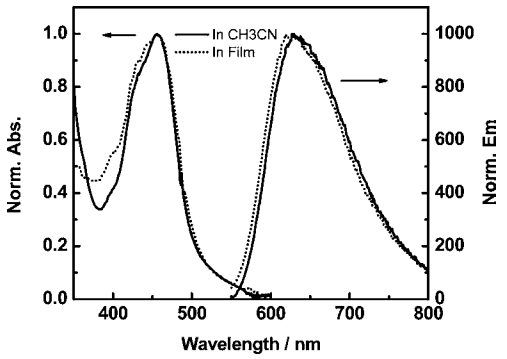

Figure 8. Absorption and corrected emission spectra of **P3** in CH_3CN (solid curves) and PEG-DMA550 film (broken curves). Excitation wavelength, 460 nm.

emission spectrum in PEG-DMA550 film showed a slight blue shift compared to the spectrum measured in CH_3CN solution while there was no significant difference in the MLCT absorption band. The blue shift in the emission spectrum compared to the spectrum in solution arises from the frozen nature of the medium. In solution, MLCT excitation is followed by solvent relaxation to a local polarization environment appropriate to the excited state dipole. In frozen media, the local polarization is largely frozen resulting in an enhanced excited-to-ground state energy gap.[26]

Figure 9 shows emission decay profiles for $Ru(bpy)_3(PF_6)_2$, monomer **4** and **P3** in PEG-DMA550 films monitored at 650

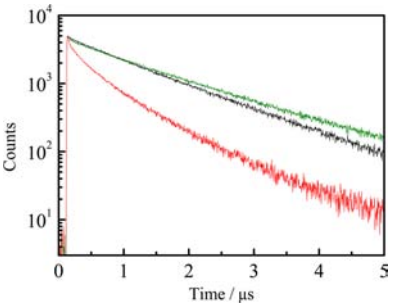

Figure 9. Emission decay profiles of $Ru(bpy)_3(PF_6)_2$ (black), monomer **4** (green), and **P3** (red) in PEG-DMA550 film: excitation wavelength = 445 nm and emission wavelength = 650 nm.

nm. The decay profile for **P3** deviates from a single, exponential decay, and the longer-lived decay component is comparable to the emission lifetime of $Ru(bpy)_3(PF_6)_2$ and monomer **4** (~1.4 μs) in CH_3CN. Nevertheless, all three samples display longer lifetimes in PEG-DMA550 films than those in CH_3CN solution. This is a manifestation of the "rigid medium effect"

dx.doi.org/10.1021/ic400520m | Inorg. Chem. 2013, 52, 8511−8520

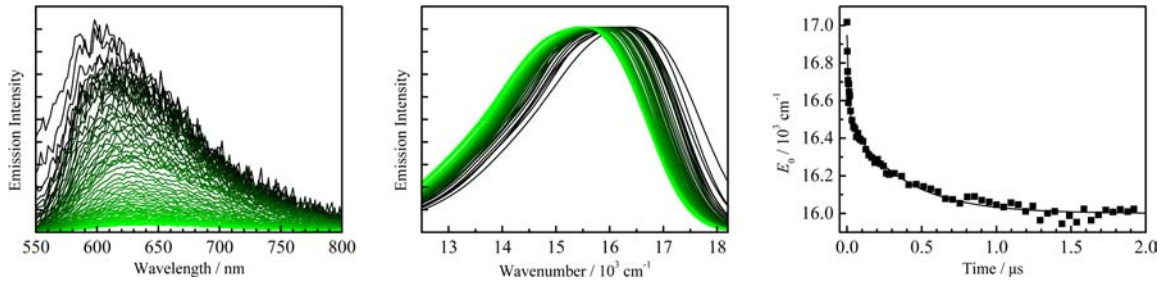

Figure 10. Corrected time-resolved emission spectra (left), normalized theoretical fits by one-mode Franck–Condon analysis (center) at 0–2 μs after the excitation (black to green), and time profile of the decrease in E_0 (right) for **P3** in PEG-DMA550 film. Excitation at 445 nm.

and the influence of the increased excited-to-ground state energy gap on nonradiative decay.[18] As discussed above, the short-lived decay component observed for **P3** represents a heterogeneous distribution of excited-state energy sites and rapid intrastrand energy migration.

We previously noted that the appearance of multi exponential kinetics in multichromophore polymers is often accompanied by time-dependent emission spectral shifts to red.[12,27] The time-resolved emission spectrum of **P3** in CH_3CN solution is shown in Supporting Information, Figure S10. These data show that the emission maximum gradually shifts from 617 to 623 nm on a 2 μs time scale without significant change in the emission profile. In comparison, Figure 10 shows the time-resolved emission spectra of **P3** in a PEG-DMA550 film. The emission spectrum gradually shifts from ~600 to ~630 nm, a larger shift than that observed in CH_3CN. At or near room temperature emission from the polymers is structureless. In fitting these spectra a one-mode, Franck–Condon analysis was used as eq 2,[28] with low frequency bpy-ring torsional and metal–ligand stretching modes treated classically and included in the bandwidth. In these fits the single mode is the average of 8–10 medium frequency υ (bpy) modes.[29] With the appearance of vibronic structure at 77 K, a two-mode fit was utilized which included both averaged medium and low-frequency modes.

$$I(\tilde{\nu}) = \sum_{m=0}^{\infty}\left(\frac{E_0 - m\hbar\omega}{E_0}\right)^3\left(\frac{S^m}{m!}\right) \exp\left[-4\ln 2\left(\frac{\tilde{\nu} - E_0 + m\hbar\omega}{\tilde{\nu}_{1/2}}\right)^2\right] \quad (2)$$

In eq 2, $I(\tilde{\nu})$ is the emission intensity at the energy $\tilde{\nu}$ in wavenumber (cm^{-1}), relative to the intensity of the 0→0 transition. E_0 is the energy gap between the zero–zero vibrational levels of the ground- and excited-states. m, $\hbar\omega$ and S are vibrational quantum number, the quantum spacing, and the Huang–Rhys factor reflecting the degree of distortion in the single, average mode as the difference in equilibrium displacements. $\tilde{\nu}_{1/2}$ is the full width at half-maximum (fwhm) for individual vibronic lines. The observed time-resolved emission spectrum at each delay time after excitation was adequately fit by eq 2 as described in our recent related paper.[30] The correlation coefficients (r) for the one-mode fits are shown, together with the fitting parameters, in the Supporting Information, Tables S2 and S3. The theoretical fits and the time profile of the E_0 value are also shown in Figure 10. From the fits, the E_0 value shifted from 17,000 to 16,000 cm^{-1} within 2 μs after excitation compared to 16200 to 16050 cm^{-1} in CH_3CN (see Supporting Information, Figure S10). These results point to a more inhomogeneous environment for **P3** in PEG-DMA550 compared to solution with significant variations of the excited-state energies and the time dependence of the emission spectrum on intrastrand energy migration to low energy sites in the frozen medium where nonradiative decay is enhanced. Based on this interpretation, the average rate constant for energy migration ($\langle k_{mig}\rangle$) was determined to be 5×10^6 s^{-1} with an average E_0 decay time of ~200 ns.

Structure Modeling by Molecular Dynamics Simulations. In terms of microscopic insight, energy transfer dynamics depend on polymer structures, and the rates vary exponentially with the distance between chromophores, in this case, distance between Ru pendants. To illustrate this point, the polymers investigated here were simulated by using 20 monomer repeat units for each of the four polymer structures (see Table 1). There are two main differences between the polymers. First, the number of pendant Ru-complexes per polymer repeat unit is varied between full loading (**P4**) vs 90% loading (**P3**) (for the latter there is a benzoic acid unit for each 9 Ru pendant units, optimized structure shown in Figure S11 in the Supporting Information). The second difference is in the length of the linker between the amino and Ru pendant unit, with methyl linker for **P3** and **P4** and ethyl linker for **P3′** and **P4′** (the latter polymers were not studied experimentally). Note that **P4′** resembles the previously studied **P2**,[4] with the only difference being the position of the amino group. All four polymers were generated and simulated according to the procedure in the Materials section. Typical structures of **P3′** and **P4′** are shown in the Supporting Information. The average nearest-neighbor Ru–Ru distances are summarized in Table 1. As can be seen in Table 1, there is interplay between linker length and higher loading that determines which specific polymer gives a shorter average nearest-neighbor Ru–Ru distance. Figure 11 compares the radial distribution function of **P3** and **P4**, and the position of the first peak in this figure represents the closest Ru–Ru distance that each polymer can reach. While **P3** (Ru–Ru nearest-neighbor average distance 10.31 Å) has a shorter Ru–Ru nearest-neighbor average distance than **P4** (Ru–Ru average distance 11.11 Å), it is also evident from the position and size of the first peak in Figure 11 that **P3** features these short distances much more frequently than **P4**, where **P3** has a closest Ru–Ru distance of ~9 Å. It is interesting to note that in most cases the nearest-neighbor pairs of Ru-pendants are not adjacent on the polystyrene backbone. Rather, in some cases they can be quite far separated along the chain. Figure S12 in the Supporting Information shows, for instance, a map of how different Ru-pendants find their nearest Ru neighbor in **P3** by plotting the arrows for the nearest

dx.doi.org/10.1021/ic400520m | Inorg. Chem. 2013, 52, 8511–8520

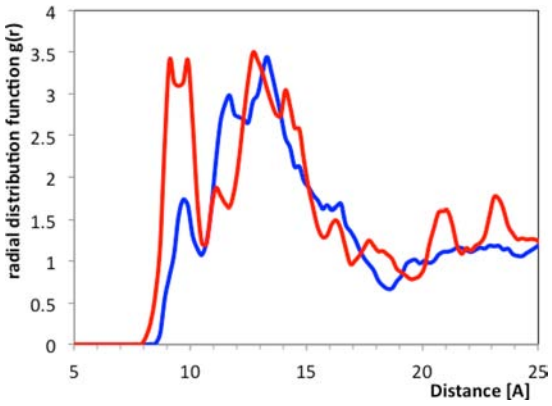

Figure 11. Calculated radial distribution function of the distance between Ru–Ru centers for **P4** (blue line) and **P3** (red line). Only distributions up to 25 Å are shown.

connections that exist for more than 50% of the snapshots from MD simulations.

We find that there is no apparent pattern in how the nearest Ru-pendant is located for any of the polymers. The average theoretically determined nearest-neighbor Ru–Ru distance and radial distribution distances calculated here (for both **P3** and **P4**) are significantly shorter than that in **P2** and Ru–Os random polymers reported previously.[1a,3] This is probably due to the differences in the computational methods employed, with previous studies assuming that $Ru(bpy)_3$ units are hard spheres, while in this work we use a full atomistic model, which allows the $Ru(bpy)_3$ units to be closer. At the same time, the differences in the polymer length and loading level of **P2** compared to **P3** or **P4** could also contribute to such observed differences. The dense loading of Ru-chromophores in **P2** causes the polymer to adopt an extended rod-like structure that alleviates the steric and Coulombic repulsions between adjacent chromophores. Meanwhile, the close proximity of the Ru pendant units in **P3** and **P4** facilitates faster energy transfer *hopping* among the Ru complexes. An experimentally measured energy transfer rate on the nanosecond time scale was observed for **P3** (see Supporting Informations, Figure S10). An important aspect of the computational results is the similarity in average Ru–Ru distance and Ru–Ru radial distribution between **P3** and **P4** even though **P3** is only 90% loaded and **P4** is 100% loaded. Based on these computational results and the Ru–Ru distances, rapid energy migration can still be achieved with lower loading of 90% as demonstrated here experimentally.

CONCLUSION

Polypyridylruthenium derivatized polystyrenes have been synthesized by ATRP with narrow PDI and moderate molecular weights, followed by derivatization by transamidation in high yields. Although a relatively short linker tethers the Ru polypyridyl units to the polystyrene backbone, a high loading level of Ru units on the polystyrene backbone was achieved. The polymers have good solubility in polar solvents, for example, DMF, THF, and CH_3CN. The polymeric chromphores show similar absorption and emission spectra compared to $Ru(bpy)_3(PF_6)_2$, indicating that there are, at best, only weak interactions between the polymer-bound chromophores, despite their close proximity. Polymer **P5**, with an electron acceptor methyl viologen (MV^{2+}) end-group exhibited a suppressed emission quantum yield and lifetime. For this polymer, intrachain energy transfer hopping to the terminal chromophore and electron transfer quenching by MV^{2+} occur. Intrastrand lifetimes are characteristic of $[Ru(bpy)_3]^{2+}$ (~1 μs), but decays are nonexponential with time-dependent emission maxima. These observations are consistent with intrastrand energy migration by Ru* to Ru hopping to low energy sites where nonradiative decay is enhanced.

Time-resolved emission spectra in rigid medium demonstrate a significant variation in the distribution of excited state energies with intrastrand migration, with the effect enhanced compared to those in solution. Following excitation, the energy gap between ground state and excited state shifts significantly from 17000 to 16000 cm^{-1} on the microsecond time scale compared to a shift of ~16200 to 16050 cm^{-1} in CH_3CN solution. The amplified effect for the polymer in the semirigid film is consistent with an enhanced heterogeneous distribution of excited state sites with rapid intrastrand energy migration between sites with a rate constant of 5×10^{-6} s^{-1}. Enhanced heterogeneity in the film compared to solution is attributed to its frozen nature in contrast to solution where rapid fluctuations lead to local equilibration. Suppression of molecular motion in the films increses the distribution of excited state sites with the energy migration among sites to low energy environments where nonradiative decay is enhanced. Calculations show that close packing of the chromophore occurs in the polymers with ~9 Å minimal Ru–Ru distances calculated by MD simulations with the relatively close contact distances supporting rapid intrastrand energy migration among the Ru chromophores.

ASSOCIATED CONTENT

Supporting Information

GPC elution curve of **6**, ^1H NMR spectra of **6**, **P3**, and **P5**, IR spectra of **6** and **P3**, excitation spectrum of **P3**, absorption spectra of **P3** upon the addition of MV^{2+}, dynamic laser scattering spectra of **P3** without and with MV^{2+}, absorption and emission spectra of **P3** upon the addition of $LiClO_4$, emission decay profiles of monomer and polymers, time-resolved emission profiles of **P3** in CH_3CN, figures of computational results, tables of spectral fitting parameters of **P3** in CH_3CN and PEG-DMA550 film. This material is available free of charge via the Internet at http://pubs.acs.org.

AUTHOR INFORMATION

Corresponding Author

*E-mail: tjmeyer@email.unc.edu.

Notes

The authors declare no competing financial interest.

ACKNOWLEDGMENTS

We acknowledge support from the UNC EFRC: Center for Solar Fuels, an Energy Frontier Research Center funded by the U.S. Department of Energy, Office of Science, Office of Basic Energy Sciences under Award Number DE-SC0001011 supporting Z.F., J.R., Z.C. and Z.W. A.I. acknowledges support from the U.S. Department of Energy, Office of Science, Office of Basic Energy Sciences, under Award Number DE-FG02-06ER15788. S.K. acknowledges support under U.S. DOE SciDAC-e award DE-FC02-06ER25764. We also acknowledge support for the purchase of instrumentation from the UNC EFRC Center for Solar Fuels (award DE-SC0001011) and from UNC SERC ("Solar Energy Research Center Instrumentation Facility" funded by the U.S. Department of Energy,

Office of Energy Efficiency & Renewable Energy, under Award Number DE-EE0003188).

REFERENCES

(1) (a) Alstrum-Acevedo, J. H.; Brennaman, M. K.; Meyer, T. J. *Inorg. Chem.* **2005**, *44*, 6802. (b) Schubert, U. S.; Eschbaumer, C. *Angew. Chem., Int. Ed.* **2002**, *41*, 2892. (c) Peng, Z.; Gharavi, A. R.; Yu, L. *J. Am. Chem. Soc.* **1997**, *119*, 4622. (d) Forster, R. J.; Vos, J. G. *Macromolecules* **1990**, *23*, 4372. (e) Aamer, K. A.; Tew, G. N. *Macromolecules* **2007**, *40*, 2737. (f) Happ, B.; Friebe, C.; Winter, A.; Hager, M. D. *Eur. Polym. J.* **2009**, *45*, 3433. (g) Liu, Y.; Jiang, S.; Schanze, K. S. *Chem. Commun.* **2003**, 650.

(2) (a) Webber, S. E. *Chem. Rev.* **1990**, *90*, 1469. (b) Meyer, T. J. *Acc. Chem. Res.* **1989**, *22*, 163.

(3) Dupray, L. M.; Devenney, M.; Striplin, D. R.; Meyer, T. J. *J. Am. Chem. Soc.* **1997**, *119*, 10243.

(4) Friesen, D. A.; Kajita, T.; Danielson, E.; Meyer, T. J. *Inorg. Chem.* **1998**, *37*, 2756.

(5) (a) Jones, W. E.; Baxter, S. M.; Strouse, G. F.; Meyer, T. J. *J. Am. Chem. Soc.* **1993**, *115*, 7363. (b) Fleming, C. N.; Dupray, L. M.; Papanikolas, J. M.; Meyer, T. J. *J. Phys. Chem. A* **2002**, *106*, 2328. (c) Sun, Y.; Chen, Z.; Puodziukynaite, E.; Jenkins, D. M.; Reynolds, J. R.; Schanze, K. S. *Macromolecules* **2012**, *45*, 2632.

(6) Meyer, T. J.; Papanikolas, J. M.; Heyer, C. M. *Catal. Lett.* **2011**, *141*, 1.

(7) Peek, B. M.; Ross, G. T.; Edwards, S. W.; Meyer, G. J.; Meyer, T. J.; Erickson, B. W. *Int. J. Pept. Protein Res.* **1991**, *38*, 114.

(8) Aamer, K. A.; Tew, G. N. *J. Polym. Sci., Part A: Polym. Chem.* **2007**, *45*, 5618.

(9) Knight, T. E.; Goldstein, A. P.; Brennaman, M. K.; Cardolaccia, T.; Pandya, A.; DeSimone, J. M.; Meyer, T. J. *J. Phys. Chem. B* **2010**, *115*, 64.

(10) (a) Suzuki, K.; Kobayashi, A.; Kaneko, S.; Takehira, K.; Yoshihara, T.; Ishida, H.; Shiina, Y.; Oishi, S.; Tobita, S. *Phys. Chem. Chem. Phys.* **2009**, *11*, 9850. (b) Ishida, H.; Tobita, S.; Hasegawa, Y.; Katoh, R.; Nozaki, K. *Coord. Chem. Rev.* **2010**, *254*, 2449.

(11) (a) Parker, C. A.; Rees, W. T. *Analyst* **1960**, *85*, 587. (b) Valeur, B. *Molecular Fluorescence: Principles and Applications*, 3rd ed., corrected reprint; Wiley-VCH: Weinheim, Germany, 2006.

(12) (a) Parr, R. G.; Yang, W. *Density-Functional Theory of Atoms and Molecules*; Oxford University Press: Oxford, U.K., 1989. (b) Becke, A. D. *J. Chem. Phys.* **1992**, *96*, 2155.

(13) (a) Hay, P. J.; Wadt, R. W. *J. Chem. Phys.* **1985**, *82*, 270. (b) Wadt, R. W.; Hay, P. J. *J. Chem. Phys.* **1985**, *82*, 284. (c) Hay, P. J.; Wadt, R. W. *J. Chem. Phys.* **1985**, *82*, 299.

(14) Frisch, M. J.; Trucks, G. W.; Schlegel, H. B.; Scuseria, G. E.; Robb, M. A.; Cheeseman, J. R.; Montgomery, J. A., Jr.; Vreven, T.; Kudin, K. N.; Burant, J. C. et al. *Gaussian 09*, revision A.1; Gaussian, Inc.: Wallingford, CT, 2009.

(15) Rappe, A. K.; Casewit, C. J.; Colwell, K. S.; Goddard, W. A., III; Skiff, W. M. *J. Am. Chem. Soc.* **1992**, *114*, 10024.

(16) Busche, C.; Comba, P.; Mayboroda, A.; Wadepohl, H. *Eur. J. Inorg. Chem.* **2010**, 1295.

(17) Coessens, V.; Pintauer, T.; Matyjaszewski, K. *Prog. Polym. Sci.* **2001**, *26*, 337.

(18) Rillema, D. P.; Allen, G.; Meyer, T. J.; Conrad, D. *Inorg. Chem.* **1983**, *22*, 1617.

(19) Kawanishi, Y.; Kitamura, N.; Tazuke, S. *Inorg. Chem.* **1989**, *28*, 2968.

(20) Feng, F.; Lee, S. H.; Cho, W. S.; Komurlu, S.; McCarley, T. D.; Roitberg, A.; Kleiman, V. D.; Schanze, K. S. *Langmuir* **2012**, *28*, 16679.

(21) Volker, J.; Klump, H. H.; Manning, G. S.; Breslauer, K. J. *J. Mol. Biol.* **2001**, *310*, 1011.

(22) Claesson, P. M.; Fielden, M. L.; Dedinaite, A.; Brown, W.; Fundin, J. *J. Phys. Chem. B* **1998**, *102*, 1270.

(23) Schlenoff, J. B.; Rmaile, A. H.; Bucur, C. B. *J. Am. Chem. Soc.* **2008**, *130*, 13589.

(24) Bock, C. R.; Meyer, T. J.; Whitten, D. G. *J. Am. Chem. Soc.* **1974**, *96*, 4710.

(25) Kim, H.-B.; Kitamura, N.; Tazuke, S. *J. Phys. Chem.* **1990**, *94*, 7401.

(26) (a) Fleming, C. N.; Brennaman, M. K.; Papanikolas, J. M.; Meyer, T. J. *Dalton Trans.* **2009**, 3903. (b) Knight, T. E.; Goldstein, A. P.; Brennaman, M. K.; Cardolaccia, T.; Pandya, A.; DeSimone, J. M.; Meyer, T. J. *J. Phys. Chem. B* **2011**, *115*, 64.

(27) Fleming, C. N.; Jang, P.; Meyer, T. J.; Papanikolas, J. M. *J. Phys. Chem. B* **2004**, *108*, 2205.

(28) Ito, A.; Meyer, T. J. *Phys. Chem. Chem. Phys.* **2012**, *14*, 13731.

(29) Thompson, D. G.; Schoonover, J. R.; Timpson, C. J.; Meyer, T. J. *J. Phys. Chem. A* **2003**, *107*, 10250.

(30) Ito, A.; Stewart, D. J.; Fang, Z.; Brennaman, M. K.; Meyer, T. J. *Proc. Natl. Acad. Sci. U.S.A.* **2012**, *109*, 15132.